Dynamics of confined cavity modes in a phononic crystal slab investigated by *in situ* time-resolved experiments

R. Marchal,[1] O. Boyko,[1] B. Bonello,[1,*] J. Zhao,[1] L. Belliard,[1] M. Oudich,[2] Y. Pennec,[2] and B. Djafari-Rouhani[2]

[1]*Institut des NanoSciences de Paris (INSP–UMR CNRS 7588) Université Pierre et Marie Curie (box 840) 4, place Jussieu 75252 Paris Cedex 05, France*

[2]*Institut d'Electronique, de Micro-électronique et de Nanotechnologie (IEMN–UMR CNRS 8520) Université Lille1, UFR de Physique, Cité Scientifique, 59652 Villeneuve d'Ascq Cedex, France*

(Received 6 September 2012; published 17 December 2012)

The confinement of elastic waves within a single defect in a phononic crystal slab is investigated both experimentally and theoretically. The structure is formed by a honeycomb lattice of air holes in a silicon plate with one hole missing in its center. The frequencies and polarizations of the localized modes in the first band gap are computed with a finite element method. A noncontact laser ultrasonic technique is used both to excite flexural Lamb waves and to monitor *in situ* the displacement field within the cavity. We report on the time evolution of confinement, which is distinct according to the symmetry of the eigenmode.

DOI: 10.1103/PhysRevB.86.224302 PACS number(s): 43.20.+g, 43.40.+s, 63.20.−e

I. INTRODUCTION

In periodic elastic structures, the main consequence of the coherent scattering, and the subsequent interferences of the scattered elastic waves, is the opening of complete phononic band gaps (i.e., frequency intervals over which propagation is forbidden, whatever the direction of the incident wave). The geometric and physical conditions for a band gap to occur have been extensively studied both theoretically and experimentally for bulk or guided waves propagating in perfect phononic crystals (PCs) made of any combination of materials.[1–8]

Altering the geometrical and/or physical properties of the perfect structure at a single point drastically changes dispersion curves since the localization in the vicinity of the defect of one or several elastic modes at frequencies in the band gap is expected. This occurrence has raised a lot of interest, not only due to the large number of possible applications (e.g., sensing, filtering, waves guiding, wavelength (de)multiplexing) but also because of the rich physics in fundamental topics, such as wave localization in inhomogeneous media or the simultaneous confinement of photons and phonons in phoxonic cavities.[9–12] Quite a few situations have been envisaged and investigated by several theoretical or experimental approaches, including calculation of the band structure,[13–15] computations of and experiments with sound transmission,[16,17] or even direct observation of the confined elastic energy.[18,19] In particular, it has been shown that a defect band opens when defects are periodically distributed in an otherwise perfect PC.[13] This defect band reduces to the degenerate state within the Bragg gap, such that neighboring defects are separated by a few unit cells. Such a resonance mode manifests itself as a sharp peak in the transmission power spectra at a frequency within the band gap. This was mainly investigated in PCs with a fluid background (i.e., supporting only bulk compression waves),[13,16,20–22] though composite structures with solid host material are of great practical importance.[18,23,24] Motivated by needs for new microelectronic components, it was proposed[25] that the confinement between free surfaces of a silicon plate be used to elaborate PC slabs with two-dimensional periodicity of similar thickness and featuring a resonant line defect in the middle. Similar to the resonant tunneling effect through a double barrier, peaks in the transmission throughout the entire structure at the resonant frequencies of the cavity are then expected and were measured in the range of hundreds of megahertz.[25] It was the first step to a better understanding of the mechanisms of sound confinement in inhomogeneous media. Our goal in this paper is to go further by addressing the confinement of elastic modes in a point defect since there have been only a few experimental studies dealing with such a defect. Besides demonstrating the existence of defect modes, we study especially the time evolution of the formation of confined states by means of *in situ* time-resolved experiments and show that the dynamics of confinement are distinct according to the symmetry of the defect modes.

II. SAMPLE AND EXPERIMENTAL DETAILS

The PC slab we used for this study was elaborated in a silicon plate with a honeycomb lattice of circular air holes drilled through the plate (see right panel in Fig. 1). The lattice constant ($a = 111\ \mu$m) was set to a value almost equal to the thickness of the plate ($t = 110\ \mu$m) in order to obtain a phononic band gap as large as possible in this PC. For the same reason, the filling ratio was fixed to about its maximum value (f $\sim$ 0.54), leaving only a few micrometers between two adjacent holes. Twenty-five and 26 rows of holes were etched along the crystallographic directions ⟨100⟩ and ⟨010⟩ of silicon, respectively, with a deep, reactive-ion etching process. The overall lateral dimensions were 1.9×2.3 mm^2. With these geometrical parameters, a complete band gap centered on 17 MHz was computed to open up in the dispersion curves between 13 and 21 MHz. The band structure of the perfect infinite system, calculated by a three-dimensional finite elements method (FEM) is shown in Fig. 1. By removing one hole in the middle of the sample, we created a vacancy-type defect forming a planar cavity in the PC. In order to ensure good confinement of potentially trapped elastic modes, this cavity was surrounded by six hexagonal cells on both sides of the cavity along x and by three cells on both sides along y.

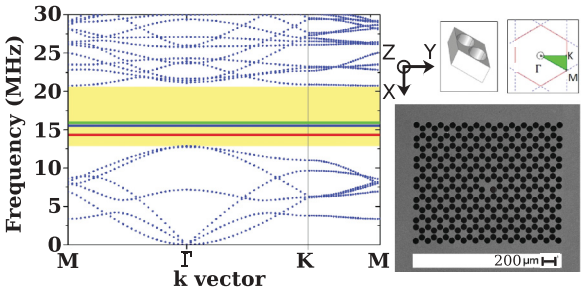

FIG. 1. (Color online) Band structure of a Si/air phononic plate with a honeycomb lattice. The thickness is $t = 110$ μm, and the lattice parameter is $a = 111$ μm. The lines in the band gap are for the eigenmodes localized within a single defect. The right panel shows a scanning electron micrograph (SEM) image of the sample, together with the unit cell used to calculate the dispersion curves.

The cavity shows fewer symmetry elements than the perfect PC: the sixfold axis normal to the plate reduces to a threefold axis, with no mirror plane parallel to the (y, z) plane, which could be a drawback for future applications. However, this geometry allows for only a small numbers of localized modes, which is an advantage in the framework of this study. This is further confirmed by an FEM analysis of the dispersion in the altered structure that shows only three defect bands in the band gap of the perfect PC at A = 15.4, B = 15.3, and C = 14.3 MHz. The three components of the displacement field associated with each of these defect modes are displayed in Fig. 2. It is important to point out here several symmetry elements in these displacement fields since selection rules could introduce some limitations in the excitation processes. Modes A and C have identical symmetries with respect to the (x,z) mirror plane (antisymmetric along x and z; symmetric along y), whereas mode B has opposite symmetries (symmetric along x and z; antisymmetric along y).

The experimental technique we used is based on laser generation and detection of acoustic pulses within a narrow spectrum.[26,27] Ultrashort light pulses of 35 ps issued from a frequency-doubled (532-nm) Q-switched Nd:YAG laser were

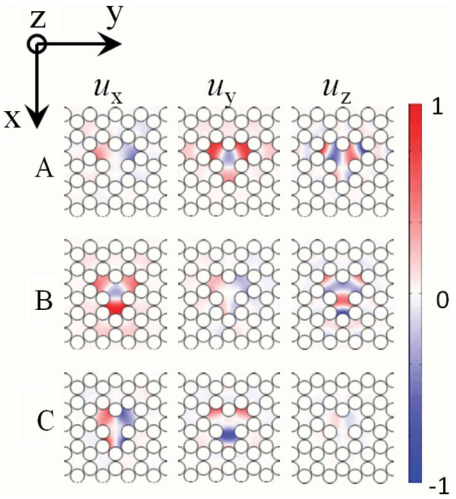

FIG. 2. (Color online) Calculated components of the displacement fields for eigenmodes: A = 15.4 MHz, B = 15.3 MHz, and C = 14.3 MHz.

focused onto the sample after they had passed through an amplitude mask and an imaging system. As a result, a series of alternately bright and dark fringes were produced, which in turn excited elastic waves owing to photoelastic processes. This technique allows the fine selection of any $\boldsymbol{k}$ vector in the Brillouin zone by tuning the spacing of the light fringes—or equivalently the wavelength of the elastic waves—with the imaging system. In all the experiments described here, laser power was kept well below the ablation threshold in order to operate in the thermoelastic regime. In this regime, we measured the maximum normal displacement in the excitation zone at ∼300 pm (i.e., about half the lattice parameter of Si). The excitation zone was located a few millimeters ahead of the PCs in a uniform region of the sample free from any air inclusion. As a result of the large number of fringes in the excitation spot and their length (∼3 mm), both the direction and the magnitude of the excited $\boldsymbol{k}$ vector were accurately defined. It should also be noted that antisymmetric Lamb waves, which have an out-of-plane component much larger than symmetric Lamb waves, are more efficiently excited by this method. The time dependence of the surface displacements was recorded at any point of the sample, inside or outside the PC, using a Michelson interferometer with a He-Ne laser light source. One beam of the interferometer was focused on the sample with a microscope objective (NA 0.42), acting as one of the mirrors of the interferometer to a spot of ∼5 μm, whereas the reference beam was reflected by an actively stabilized mirror. Both mirrors were finely set to achieve the optical contact and uniform intensity pattern, yielding a maximum contrast of 0.92. A loop feedback device allowed the setting of optical path differences to $\lambda/4$ (modulo λ), therefore achieving optimum sensitivity and a linear response to the normal displacements at the surface of the sample. The microscope and the sample were both mounted on translation stages in such a way that the probe beam could be scanned across the sample over a maximum area of 25 × 25 mm^2, with absolute and relative precisions of ∼10 and ∼1 μm, respectively. The interference pattern was collected by a high-speed photodiode and digitized at 500 MS s^{-1} by a digital oscilloscope. The frequency response of the device was flat between 20 kHz and the cutoff frequency of the photodiode, set to 50 MHz. This noncontact technique allowed us to record the displacement field at any point at the surface of the sample and hence resolve fine details of the interaction between the acoustic waves with the PC and the cavity. Note that this interferometric method is only sensitive to the normal component of the displacements, not to the in-plane components.

III. RESULTS AND ANALYSIS

We excited the zero-order antisymmetric Lamb mode A_0 over a narrow band of frequencies centered on 15 MHz close to eigenmodes A and B, and we measured the normal displacements as a function of time at several points inside and outside the PC. In a first set of experiments, the excitation area was located in the homogeneous part of the sample above P_1 (see Fig. 3). As expected for elastic waves at frequencies in the forbidden band, a strong reduction of their amplitude was observed when measurements were made inside the PC: a peak-to-peak amplitude of ∼100 pm just before the elastic

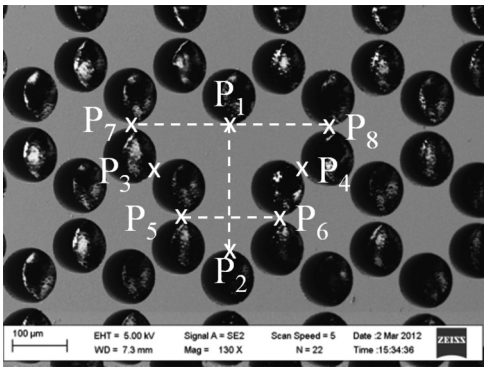

FIG. 3. SEM top view of the cavity in a Si/air phononic plate with honeycomb lattice. The dashed lines and crosses indicate the regions where measurements were made.

waves encountered the PC reduced drastically while traveling inside the PC. The amplitude was still ∼15 pm, which was well above the noise floor when measured at point P_1, where the waves enter the cavity. However, amplitude does not decrease monotonically along the path to P_1. Our simulation results as well as our measurements show that the center of each hexagonal cell is a node of vibration, whereas the thin bridges between two adjacent holes over-vibrate.

We recorded the time dependence of the out-of-plane displacements, u_z, every 5 μm within the defect between points P_1 and P_2, 220 μm apart from each other. The results are displayed in Fig. 4(a), where we show the normal component of the displacements in a time-position plot. Along the time axis, the main feature is a fast oscillation around the position of equilibrium with a period of ∼70 ns, corresponding to a vibration at 14 MHz, slightly less than the frequency of mode B. Along the space axis, three antinodes are clearly observable. The greatest amplitude of about 15 pm arises near P_1 and P_2, and it reduces to ∼7 pm for the antinode in the center of the cavity. These maxima are separated from one another by nodes where the membrane is at rest. The relative amplitudes of these maxima are in good agreement with the computations of the component u_z of mode B shown in Fig. 2. Furthermore, the top view displayed in Fig. 4(b) confirms the forming of a standing wave in the cavity, which allows the related dynamics to be studied. In addition the phase of the standing wave along the line joining P_1 and P_2 matches that of mode B [see Fig. 4(c)], which appears to be the only mode excited in this experimental configuration. This period, lasting from ∼0.2 to ∼1.8 μs, during which the waves remain confined in the cavity, is surrounded by episodes in which waves propagate from P_1 to P_2 or from P_2 to P_1, as can be inferred from the slopes of the equiphase lines in the time-position plot [see the full lines in Fig. 4(b)]. Moreover, this is consistent with the symmetry of the source, which might not excite this mode if it has no symmetry elements in common with it, as is the case for modes A and C.

It is also interesting to point out in Fig. 4(b) the moments when the maxima of vibration come up: although the wave enters the cavity at point P_1, an antinode first settles near P_2 on the opposite side of the cavity. The antinode near P_1 takes place ∼0.2 μs later [see arrows in Fig. 4(b)]. This delay is easily understood by noting that the acoustic mode trapped

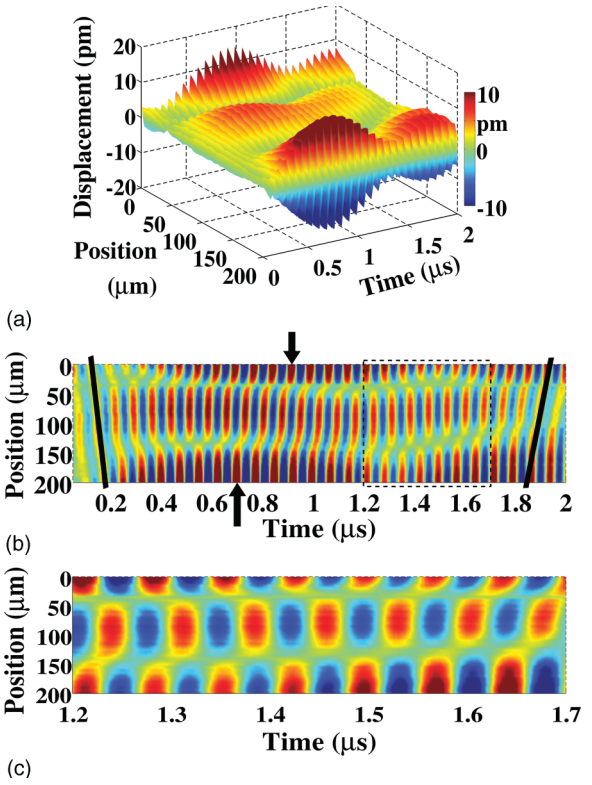

FIG. 4. (Color online) (a) Normal component of the displacement field inside the cavity in a time-position plot. The signal was recorded along the line joining P_1 (0 in the position axis) to P_2 (200 in the position axis). The frequency of the zero-order flexural Lamb mode is tuned to 15 MHz. (b) Top view of the data displayed in panel (a). The arrows are for the maximum of the antinodes located near P_1 and P_2. The full lines are guides to the eyes showing propagating waves. (c) Zoom of the data in the area delimited by a dashed line in panel (b) showing standing waves in the cavity (mode B).

in the cavity originates from the interference of the incident wave with itself after it has been partly reflected in P_2 to form a standing wave in the cavity [Fig. 4(c)]. Another fundamentally important aspect of these experimental results relates to the spectrum of the confined mode. While the spectrum of the excitation pulse extends over about 5 MHz, a Fourier transform of the signal recorded on any of the three antinodes inside the cavity features a sharp peak of ∼0.45 MHz width and centered on 14 MHz (Fig. 5), instead of 15.3 MHz as expected from the numerical simulations. The same deviation from theory was measured for mode A (see below); we attribute this discrepancy to imperfections in the sample dimensions.

Quality factor Q, defined as the ratio of the eigenfrequency over the width of the Fourier component at half maximum, is commonly used to describe the quality of the resonance. It must be stressed here that the experimental procedure we used for this work is not appropriate for estimating the Q factor accurately. Because the excited wave is not a pure continuous sine at frequency ν_B of mode B, the edges of the cavity are deformed by the elastic energy associated with all the spectral components different from ν_B, in turn causing leakage of the confined mode.

To further investigate the confinement dynamics of this mode, we measured the vibrations at points P_3 and P_4 in

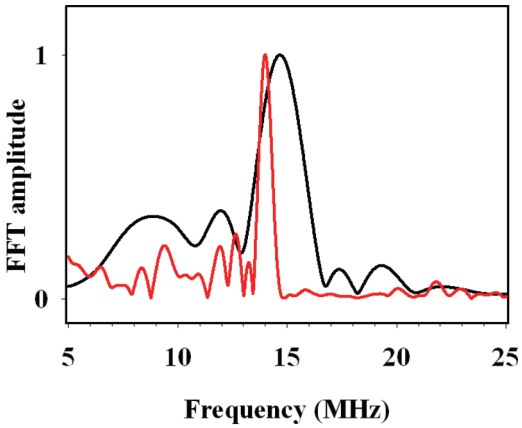

FIG. 5. (Color online) Normalized Fourier spectra of the excitation pulse (black line) and of the confined mode measured at the antinode inside the cavity.

the middle of the cavity. While FEM simulations predict that both parts of the cavity vibrate in phase with P_1 (see Fig. 2), an out-of-phase movement was observed instead for $\sim$1.2 μs after the confinement mechanism started. Following this period, the in-phase movement was observed, as expected from the simulations. This duration corresponds to that of the first antinode appearing along the time axis in Fig. 4(a). Additionally, it is interesting to notice that the delay of 1.5 μs also corresponds to the time necessary for the node initially positioned at $\sim$130 μm from P_1 to shift toward $\sim$140 μm, in a position closer to P_2. This latter position is in good agreement with the value deduced from our simulations displayed in Fig. 2. Similar measurements performed in P_5 and P_6 did not show any delay in the phase settling, which further confirms that the localization process first takes place in the lower part of the cavity.

For comparison, we show in Fig. 6 the signal recorded along the line P_1 to P_2 with identical experimental conditions, except the frequency of the excitation pulse, which was tuned to 3 MHz, a value in the first band of the antisymmetric Lamb mode A_0. At this frequency, the system behaves as an effective medium and, as it should, the antisymmetric Lamb mode propagates through the cavity at 2000 m s^{-1}, in very good agreement with the velocity deduced from the dispersion curves in Fig. 1, without any indication of confinement.

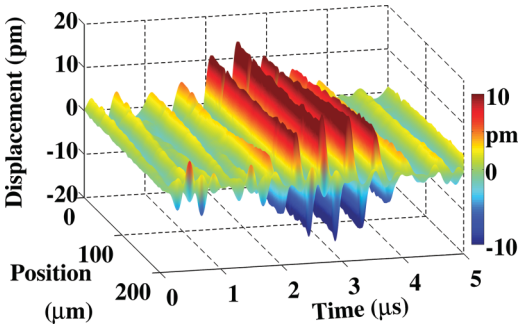

FIG. 6. (Color online) Normal component of the displacement field inside the cavity in a time-position plot. The signal was recorded along the line P_1–P_2. The frequency of the zero-order flexural Lamb mode is tuned to 3 MHz.

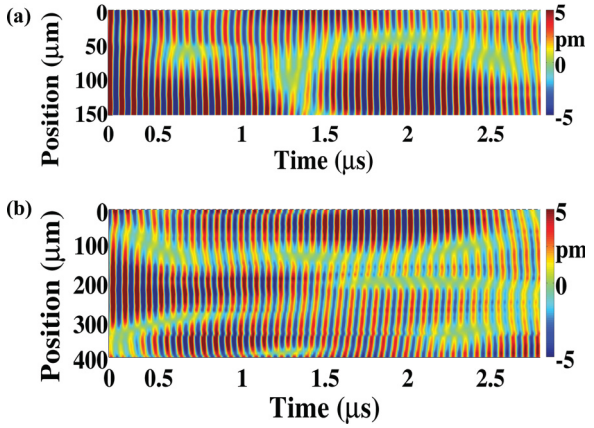

FIG. 7. (Color online) Top view of the normal component of the displacement field inside the cavity in a time-position plot. The frequency of the zero-order flexural Lamb mode is 15 MHz. The signals were recorded along the lines P_5–P_6 (a) and P_7–P_8 (b). The time origin is set to the time the elastic waves enter the cavity.

Instead, oscillations with a period of 0.3 μs are observed along the time axis.

In another set of experiments, the sample was excited laterally, and the elastic response was recorded along the lines joining P_5 to P_6 and P_7 to P_8 (Fig. 3). Because of the symmetry of the source, only mode A is expected to be excited in that case. As explained above, the Lamb mode A_0 is more efficiently excited by our thermoelastic source than is the mode S_0; mode C being symmetric with respect to the midplane of the sample, it cannot be excited by A0. Additionally, because its normal component u_z^C is one order of magnitude less than u_z^A, it is not likely to be detectable with our experimental setup. Top views of the normal displacements as a function of time, along both these lines, are shown in Fig. 7(a) and 7(b), respectively. The confinement dynamics for this mode appears to be much more complex than it is for mode B. Our measurements [Fig. 7(a)] show that the confinement first begins within the narrowest part of the cavity, where mode A features one antinode on each side of a single node line: both amplitude and phase of the vibration are consistent with what is predicted by FEM calculations. However, Fig. 7(a) reveals some fluctuations in the position of the node line, which stabilizes on its final position $\sim$2.5 μs after the waves have entered the cavity. These fluctuations are even more clearly seen in the wider part of the cavity [Fig. 7(b)]. Whereas the node lines and the antinodes near P_7 and P_8 set up with the right phases almost immediately, these fluctuations prevent the antinodes on either side of central node line to emerge for $\sim$2.5 μs. The confinement process then completes during a short time that must be related to the finite duration of the excitation pulse.

IV. CONCLUSION

In summary, we reported here *in situ* measurements of the defect modes confined in a point defect inserted in a two-dimensional PC, which allowed us to gain insight into the dynamics of PC cavity–mode localization. These results, combined with our theoretical predictions, describe how the

spatial distribution of eigenmodes depends on the symmetry of the defect and the geometry of excitation. In particular, we have shown that an eigenmode can be selectively excited by a proper choice of source position. For both modes, we investigated the overall dynamics and found that it is mainly governed by the time necessary for the standing waves to stabilize in the widest part of the cavity (area above the line P_3–P_4 in Fig. 3) because the localization process first occurs in the lower part of the cavity. By advancing the level of understanding of wavelength-scale ultrasonic phenomena, our result, at the same time, has important implications for surface acoustic wave and opto-acoustic technologies.

ACKNOWLEDGMENTS

This work is a part of Future and Emerging Technologies–Open project, Tailphox, supported by the European Community under grant 233883, and of project Metactif, supported by the Agence Nationale de la Recherche and Direction générale de l'armement under grant ANR-11-ASTR-015. The sample has been elaborated in the MIMENTO-Femto-ST clean room.

*bernard.bonello@insp.jussieu.fr

[1] M. S. Kushwaha, P. Halevi, L. Dobrzynski, and B. Djafari-Rouhani, Phys. Rev. Lett. **71**, 2022 (1993).
[2] M. M. Sigalas and E. N. Economou, Solid State Commun. **86**, 141 (1993).
[3] L. Ye, G. Cody, M. Zhou, P. Sheng, and A. N. Norris, Phys. Rev. Lett. **69**, 3080 (1992).
[4] F. R. Montero de Espinosa, E. Jimenez, and M. Torres, Phys. Rev. Lett. **80**, 1208 (1998).
[5] M. Wilm, A. Khelif, S. Ballandras, V. Laude, and B. Djafari-Rouhani, Phys. Rev. E **67**, 065602(R) (2003).
[6] C. Charles, B. Bonello, and F. Ganot, Ultrasonics **44**, e1209 (2006).
[7] T.-T. Wu and Z.-G. Huang, Phys. Rev. B **70**, 214304 (2004).
[8] B. Bonello, C. Charles, and F. Ganot, Appl. Phys. Lett. **90**, 021909 (2007).
[9] M. Maldovan and E. Thomas, Appl. Phys. Lett. **88**, 251907 (2006).
[10] N. Papanikolaou, I. E. Psarobas, and N. Stephanou, Appl. Phys. Lett. **96**, 231917 (2010).
[11] Y. Pennec, B. Djafari Rouhani, E. H. El Boudouti, C. Li, Y. El Hassouani, J. O. Vasseur, N. Papanikolaou, S. Benchabane, V. Laude, and A. Martinez, Opt. Express **18**, 14301 (2010).
[12] S. Mohammadi, A. A. Eftekhar, A. Khelif, and A. Adibi, Opt. Express **18**, 9164 (2010).
[13] M. M. Sigalas, J. Appl. Phys. **84**, 3026 (1998).
[14] X. Li and Z. Liu, Sol. State Com. **133**, 397 (2005).
[15] D. Caballero, J. Sánchez-Dehesa, R. Martínez-Sala, C. Rubio, J. V. Sánchez-Pérez, L. Sanchis, and F. Meseguer, Phys. Rev. B **64**, 064303 (2001).
[16] A. Khelif, A. Choujaa, B. Djafari-Rouhani, M. Wilm, S. Ballandras, and V. Laude, Phys. Rev. B **68**, 214301 (2003).
[17] R. H. Olsson III, I. F. El-Kady, M. F. Su, M. R. Tuck, and J. G. Fleming, Sens. Actuators A **145**, 87 (2008).
[18] M. Torres, F. R. Montero de Espinosa, D. Garcia-Pablos, and N. Garcia, Phys. Rev. Lett. **82**, 3054 (1999).
[19] F. Li, J. Liu, and Y. Wu, J. Appl. Phys. **109**, 124907 (2011).
[20] A. Khelif, B. Djafari-Rouhani, J. O. Vasseur, P. A. Deymier, Ph. Lambin, and L. Dobrzynski, Phys. Rev. B **65**, 174308 (2002).
[21] X. Zhang, Z. Liu, Y. Liu, and F. Wu, Solid. State Com. **130**, 67 (2004).
[22] T.-T. Wu, C.-H. Hsu, and J.-H. Sun, Appl. Phys. Lett. **89**, 171912 (2006).
[23] M. M. Sigalas, J. Acoust. Soc. Am. **101**, 1256 (1997).
[24] I. E. Psarobas, N. Stefanou, and A. Modinos, Phys. Rev. B **62**, 5536 (2000).
[25] S. Mohammadi, A. A. Eftekhar, W. D. Hunt, and A. Adibi, Appl. Phys. Lett. **94**, 051906 (2009).
[26] T. Brunet, J. Vasseur, B. Bonello, B. Djafari-Rouhani, and A.-C. Hladky-Hennion, J. Appl. Phys. **104**, 043506 (2008).
[27] J. Pierre, O. Boyko, L. Belliard, J. O. Vasseur, and B. Bonello, Appl. Phys. Lett. **97**, 121919 (2010).